Available online at www.sciencedirect.com
SCIENCE DIRECT®
Journal of the European Ceramic Society 25 (2005) 13–18
www.elsevier.com/locate/jeurceramsoc

Electrical behaviour at high voltage on surface of SiC-β′-SiAlON ceramic composites

A. Jankowiak [a], F. Collardey [b], P. Blanchart [a,*]

[a] *GEMH, ENSCI, 87065 Limoges, France*
[b] *ENSCPB, 33607 Pessac Cedex, France*

Received 26 October 2003; received in revised form 12 February 2004; accepted 21 February 2004
Available online 19 May 2004

Abstract

This study describes the electrical behaviour of SiC-β′-SiAlON particulate composite materials under pulsed high electric fields. If such composite materials present interesting mechanical and thermal behaviour at high temperature, they also display enhanced discharges on the surface when a high electric field is applied. The global electric field required for the discharge is much reduced compared to those for similar air gaps at the same atmosphere pressure. Furthermore, the electric field required for discharge varies weakly over a large range of the atmosphere pressure. Such composite materials can be used for electric devices, where a local high energy level at high temperature is necessary. It is shown that the electrical discharge proceeds in successive steps, the first one being the local ionisation of the air atmosphere. During this step, the mechanisms involved follows Paschen's law at the microscopic scale for gaps between conductive SiC grains, but also at the macroscopic scale for the electrode gap. When the air pressure increases, a departure from Paschen's law is observed and a mechanism of breakdown is proposed based on Fowler–Nordheim's law for field emission at thin SiC grain boundaries.

Keywords: Composites; Surfaces; Electrical properties; Sialons; SiC; Breakdown

1. Introduction

Most applications for particle-reinforced ceramic matrix composites exploit their fracture toughness and their reliability for structural applications.[1] Wear resistance and toughness are also enhanced by the dispersion of hard particles in a ceramic matrix.[2] This study, in contrast, concerns the electrical properties of sintered particle-reinforced composites containing a dispersion of particles that weakly react with the matrix material. In general, these materials are metal–ceramic matrix composites, such as nickel particles in an alumina or zirconia matrix.[3] These materials can be used for electrodes in electrochemical devices, machined by electric discharge or electrochemical methods and used in electrotechnical applications. Besides the electrical properties, such ceramic materials display attractive oxidation resistance at high temperature and excellent transient thermal shock resistance.

To increase the electrical conductivity of particle-reinforced ceramic matrix composites, not only particles of metal but also particles of conductive ceramic can be used. The most competitive material is SiC, and various carbide or nitride materials can be also added. In general, the electrical behaviour is explained by the current percolation between the conductive grains. A contribution of the microstructure has also been found,[4] involving the random or uniform distribution of conductive grains and the grain boundary behaviour where secondary phases can locally modify the electrical resistance.

With such composite materials, when the conductive grain to matrix phase ratio is within a narrow range close to that for current percolation, high electric fields create electrical surface discharges. One of the most interesting aspect is the very large range of current–voltage characteristics, as compared to semiconductor devices.

The electrical discharges occur with a high energy level between the two electrodes for the electrical connection. The

* Corresponding author. Tel.: +33-5-55-45-22-22; fax: +33-5-55-79-09-98.
E-mail address: p.blanchart@ensci.fr (P. Blanchart).

0955-2219/$ – see front matter © 2004 Elsevier Ltd. All rights reserved.
doi:10.1016/j.jeurceramsoc.2004.02.003

main behaviour of this specific device is related to the variation of the breakdown voltage with gas pressure. Whereas for an air gap between isolated electrodes the variation is large, a promising feature is the flat characteristic of voltage against gas pressure. Such behaviour is useful when electrical discharges are involved in engineering applications with a high energy level at high temperature.

Our approach in this paper is to prepare particle-reinforced ceramic matrix composites using micro-sized SiC grains as conductive phase and β′-SiAlON as matrix phase, to obtain a significant oxidation resistance at high temperature. For both phases, thermal expansion coefficients are similar and thermal mismatches are therefore limited. In such a way, the thermal stress from electrical discharge is minimised, despite the high energy level of the discharge. Our ceramic matrix composites were subjected to electrical discharges and the current versus tension characteristics were recorded against the gas pressure, to investigate the mechanisms involved.

2. Experimental

A β′-SiAlON matrix material was prepared from powders Si_3N_4 (Starck, M11), Al_2O_3 (Pechiney, P172) and MgO (Prolabo) as sintering additive. The powders were firstly ball milled in water-dispersant solution (Dolapix A92, Zschimmer & Schwarz) in alumina jars with alumina balls, for 45 min. The slip density was adjusted to avoid settling, but to maintain a sufficient low viscosity to allow an intimate mixing of powders. In a second stage, SiC powder (Goodfellow) was added in slips with an organic binder (PEG 300, Prolabo), at the same time, to avoid the rapid segregation of larger SiC grains. Time and grinding energy, as the slip rheology during the mixing stage were carefully controlled to limit the reduction of SiC grain size, but to ensure the distribution of SiC grains in the matrix material. Slurries were dried in a vacuum rotary dryer at 100 °C and sieved at 500 μm to break up agglomerates. Square (7 mm × 7 mm × 5 mm) samples were shaped by isostatic compaction at 200 MPa in silicon rubber moulds. The preliminary firing stage was at low temperature (500 °C and 10 °C/h) under air, to remove organic additives. The sintering stage was in a graphite kiln at 1680 °C, under N_2 at atmospheric pressure.

Material porosity with SiC to β′-SiAlON matrix ratio are reported in Table 1, where it is seen that the overall open porosity varies slightly, although the SiC content changes significantly. The increase of porosity compensates the increase of SiC content to maintain the global density of material in a narrow range (Table 1). In Table 2, phase analyses by X-ray and individual dc electrical conductivities of SiC and β′-SiAlON sintered material are indicated. Conductivity data of SiC are reported from the supplier and β′-SiAlON data were measured by the four probe method applied to monolithic material. In Table 3, the global conductivity of composites increase with SiC content, but values are always very small. It results from the porosity of the matrix material and the very limited current percolation between SiC grains.

Table 1
Porosity, density and sintered density against SiC to β′-SiAlON matrix ratio

	SiC (vol.%)			
	51	61	65	68
Open porosity (vol.%)	23	25	27	30
Density	2.41	2.38	2.33	2.25
Relative density (%)	72.0	71.8	70.5	68.6

Table 2
Crystallographic phase and electrical conductivity at room temperature of SiC and β′-SiAlON sintered material

	Phase	Conductivity (S/cm)
SiC	α	2.43
β′-SiAlON	$Si_6Al_{10}O_2N_{14}$	1.47×10^{-13}

Table 3
Conductivities of composites against SiC to matrix phase volume ratio

	SiC (vol.%)			
	51	61	65	68
Conductivity (10^{-8} S/cm)	1.39	1.47	1.67	1.96

In the electrical discharge circuit, the energy is stored in a high voltage capacitance connected to our device through a trigger circuit and a series resistor. The electrical discharge characteristics depend not only on the device where discharges occur, but also on the electrical circuit parameters. Electronic components must be carefully chosen to obtain smooth and repeatable voltage and current histories for the discharge. By so doing, the discharge duration can be controlled. The discharge voltage and current can be directly measured using a large bandwidth oscilloscope. In our experiments, the capacitive discharge circuit is electronically switched to the ceramic device thought a damping resistor placed in series. This resistor was adjusted to avoid high frequency oscillations of the discharge current, but also to set the duration of the electrical discharge. Voltage and current were recorded via appropriate probes by a 100 MHz digital storage oscilloscope (Agilent Mega 200 M).

3. Results

The current–voltage characteristic of our composite material extends to a broad range of voltage and current, about 800 V and 300 A. The general aspect of curves is similar for all materials and two examples of experimental plots are presented in Fig. 1 for the 65 vol.% sample for two air pressures (75–750 Torr). In general, a first and rapid increases of voltage is followed by a plateau, where the voltage maximum

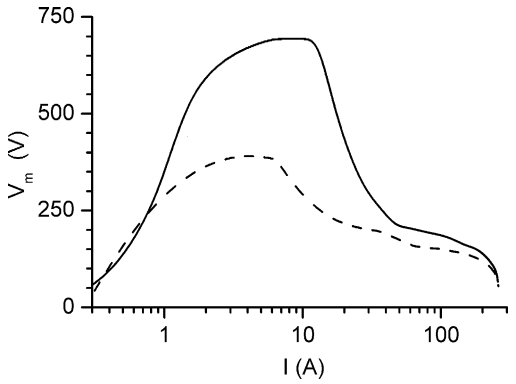

Fig. 1. Current–voltage characteristic of the sample containing 65 vol.% of SiC grains, at two air pressures 100 mbar (dashed line) and 1000 mbar (solid line).

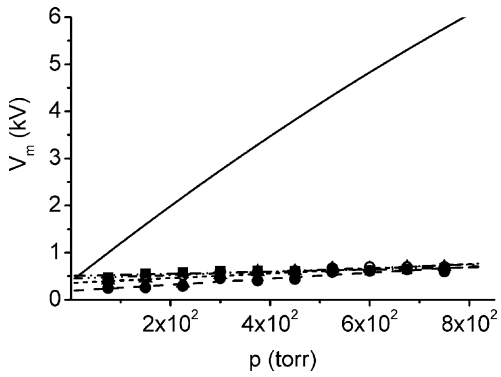

Fig. 3. V_m peak voltage of samples against the air pressure, for all samples (dashed line) and for a 1.2 mm gap between electrodes (solid line).

V_m is attained. A very rapid decrease of voltage is accompanied by the current increase. During this stage, a second and small voltage characteristic point is observed, followed by a second rapid decrease. This final stage is characterised by very large values of current. The whole duration of discharges is about 110 μs. The process ends when the capacitor discharge is exhausted, but the whole duration of the discharge was adjusted by the capacitance and the damping resistor values, to limit peaks of current and residual high frequency oscillations in the discharge current.

The macroscopic behaviour of our materials with an electrode gap of 1.2 mm was studied with peak voltage V_m against the SiC to matrix phase ratio and the air pressure. Fig. 2 presents the very weak variation of V_m against the SiC content. Fig. 3 shows that V_m values slightly increase when the air pressure changes from 75 to 750 Torr, but in Fig. 3 the V_m data for the same air gap are also plotted,[5] indicating very larger variations with air pressure.

The typical aspect of sample microstructures is presented in Fig. 4, where dense SiC grains differ from the porous matrix phase. The general aspect of all samples are similar although the SiC content changes significantly and the mixing process ensure that SiC grains are well dispersed in the matrix phase. Whereas the grain size distribution of SiC grains is already known, we were mainly interested in the SiC repartition. We measured the distance distribution between grains by image analysis of several electronic images of each sample by SEM (Hitachi S2500). Images were processed by numerical methods implemented in the *Aphelion* software (ADCIS SA, Hérouville Saint-Clair, France). As the analysis was performed with particulate materials, investigations are essentially concerned by the external shape of grains, so a preliminary chemical treatment was performed by HF etching, to increase the morphological contrast of SiC grains embedded in the matrix. Such surfaces are very suitable for SEM observations and further numerical treatments because they easily be analysed as 2D silhouette of particles.

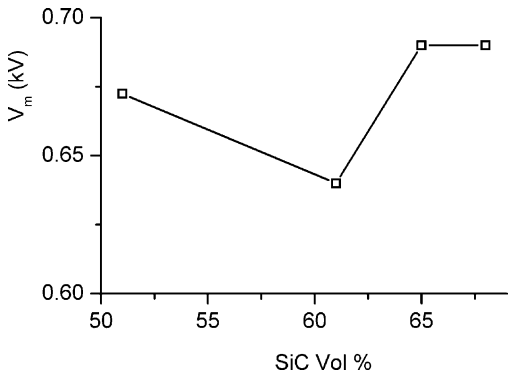

Fig. 2. V_m peak voltage of samples against SiC grains content, for a 1.2 mm gap between electrodes.

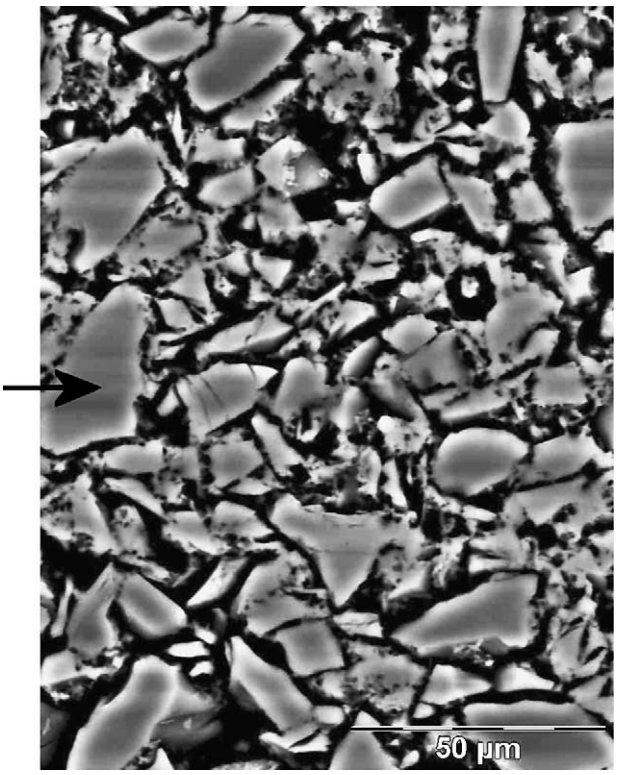

Fig. 4. SEM microstructures of a sample with 65 vol.% of SiC. The arrow indicates a dense SiC grain embedded in the porous matrix phase.

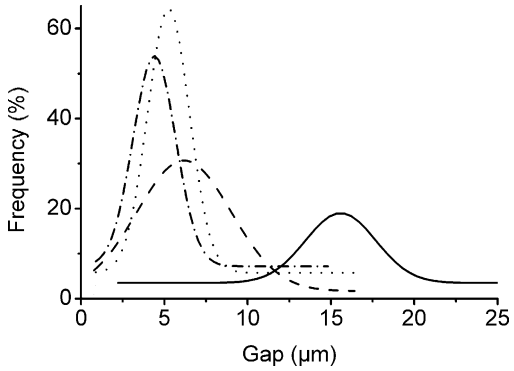

Fig. 5. Distribution functions of distances for samples containing 51 vol.% (solid), 61 vol.% (dash), 65 vol.% (dot), 68 vol.% (dash dot).

The image processing was performed following methods described in Refs. 6,7 to obtain stereological parameters describing material characteristics. Results of distribution functions of distances between nearest neighbours are presented in Fig. 5 for all samples. Distance distributions tend to shift toward lower values as the SiC volume increases, whereas the granulometry distribution of SiC grains remains very similar for all samples and unchanged from the initial size repartition.

4. Discussion

The typical current–voltage characteristic of a gas discharge at low pressure is in Fig. 6. It is interesting to note that the general aspect of this curve is similar to the *I–V* curves of our samples, in Fig. 1. Both curves extend to broad ranges of voltage and current and they present three distinguishable regions. At low current (region A in Fig. 6) is the Townsend region. The ionisation of gas molecules at the anode leads to a subsequent secondary emission at the cathode under the ion motion. The secondary emission process

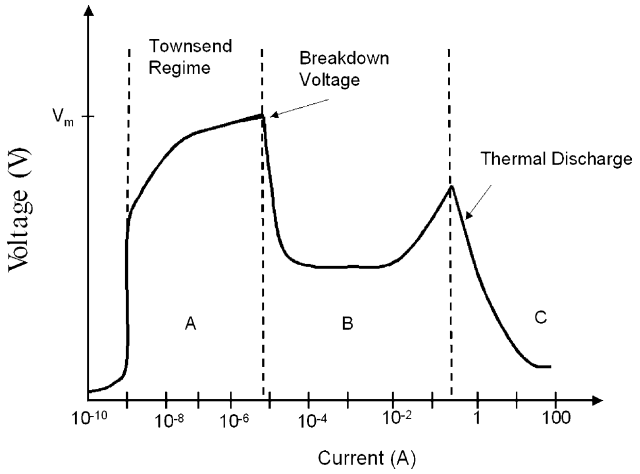

Fig. 6. Typical current–voltage characteristic for a gas discharge at low pressure.

results in the multiplication of electron emission, which becomes self-sustaining. Above the breakdown voltage (V_m), the voltage decreases and the current highly increases towards the glow region (region B) where cold plasma conditions exist. There is still a great fraction of electrons with sufficient energy to excite electronic states, to produce ions. Following this region, a slight increase of voltage indicates a further secondary emission of energetic electrons from the cathode. This phenomenon entails a transition from the glow plasma region to the thermal discharge region, which is the later discharge phase (region C). Highly conductive channels of electrons and ions form, which bridge the gap between the anode and the cathode. This high conductivity causes the local electric field to collapse to lower values, leading to a large decrease of electron energy, which no longer ionises molecules but heats the gas. The high ion and electron density within the arc results in emission of light and acoustic waves and accelerated erosion of surrounding material or electrodes.

It is firstly proposed that the electrical sequence phenomena can be explained using knowledge from electric discharges in low pressure gas, under the Paschen's law.[8,9] This model reflects the electrical breakdown mechanism in gases at the V_m voltage. V_m is related to the *pd* product, where *p* is the gas pressure and *d* is the gap between electrodes:

$$V_m = \frac{Bpd}{\ln(Apd) - \ln(\alpha d)} \quad (1)$$

where *A* and *B* are gas dependant parameters. α is the significant Townsend's first ionisation coefficient, which relates the mean free path for electron secondary ionisation to the total scattering path. It is pressure and electric field dependant.

In the continuation of the discharge process, the acceleration of ions in the electric field leads to secondary electron emissions at the electrodes. This secondary emission replenishes the population of ions and the discharge becomes self-sustaining when:

$$\alpha d = \ln\left(1 + \frac{1}{\gamma}\right) \quad (2)$$

where γ is the secondary ionisation coefficient for the electrode surface.

To assess the microscopic behaviour of our composite materials, we used the Paschen's law at gaps between the SiC grains on the material surfaces. The Paschen's law must be rewritten as:

$$\ln(p) = \frac{Bp}{E} + \ln\left(\frac{\alpha}{A}\right) \quad (3)$$

where *E* is the local electric field and a plot of $\ln(p)$ against p/E should give a straight line and α values are obtained since *A* and *B* are known from the literature.[10] Whereas the local *E* varies with gap lengths, when applied to mean values from Fig. 5, it gives quasi straight lines as shown in Fig. 7 which suggest a possible application of the Paschen's

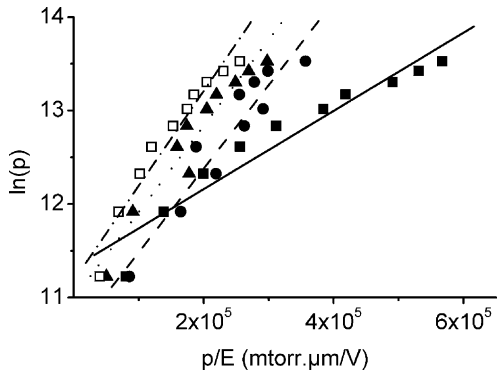

Fig. 7. Plot of ln(p) against p/E, from the Paschen's law, when the SiC content varies. SiC (vol.%): 51 (solid), 61 (dash), 65 (dot), 68 (dash dot).

model. In that way the limiting value of α at very low pressure is obtained. Furthermore, a very particular behaviour is observed when plotting Eq. (3), but at the macroscopic scale between the electrode gap (1.2 mm). It gives very similar straight lines with the same α limiting values as for the microscopic behaviour. This interesting observation supports the existence of larger ionised zones between electrodes than localised zones at micron sized gaps between SiC grains. The material response during the electrical discharge must be rather considered as a global surface phenomenon, than as a percolation phenomenon from gap to gap.

When p increases, α varies from the limiting low-pressure. Using Eq. (1), α values are reported in Fig. 8 against p/E. It shows that α decreases sharply with pressure to electric field ratio. α is the number of electron–ion pairs generated per unit distance, which is related to the secondary electron emission γ at the cathode through Eq. (2). A large decrease of α means an increase of γ, which exceeds therefore realistic values.

At micro gaps, the Paschen's law supposes that fewer ionisable molecules lead to a higher breakdown voltage. Some authors reported that the breakdown threshold changes from ideality when gaps are below a few micrometers[11,12] as is the case of several gaps in the microstructure of our samples (Fig. 4). Such behaviours will also cast some doubts in the single description by Paschen's law of electrical discharges and a further mechanism is therefore proposed.

When field emission is assumed as the main mechanism for current flowing between electrodes, the most widely used model for current flowing between electrodes is the Fowler–Nordheim's law.[13] Given the height of the potential barrier for electrons to escape from the electrode surface and the work function Φ under the electric field E, the current density j is:

$$j = \frac{aE^2}{\Phi}\exp\left(-b\frac{\Phi^{3/2}}{E}\right) \quad (4)$$

a and b depend on Φ and the work function for SiC is in a similar range as that for metals (2.7–3.5 eV).[14] a and b can be estimated as:[15]

$$a = 1.54 \times 10^{-6}\,\mathrm{A/m^2}, \quad b = 6.83 \times 10^{-9}\,\mathrm{V^{-1/2}\,m}$$

Experimentally, a good check of the field emission mechanism is obtained when the plot of $\log(I/E^2)$ versus $1/E$ gives a straight line during the pre-breakdown voltage period. The above description describes an ideal situation with perfect electrode surface. For less well characterised electrode surface, the phenomenology appears to be different.[16,17] An enhanced field emission is observed with significant current values even at low electric fields. It seems that the current emission is enhanced by local microscopic emitting sites, which can be micro-protrusions on surfaces[18] or chemically modified surfaces by doping or local deposits.

In that case, there is still a linear relationship between $\log(I/E^2)$ and $1/E$, but we have to account with an enhanced local electric field by a factor β, whereas Φ for the emitting site is supposed to be unchanged. Eq. (4) becomes:

$$j = \frac{a\beta^2E^2}{\Phi}\exp\left(-b\frac{\Phi^{3/2}}{\beta E}\right) \quad (5)$$

The experimental plot of $\log(I/E^2)$ versus $1/E$ is in Fig. 9 for one sample, for the discharge period just before the breakdown voltage. It is seen that during the pre-breakdown voltage situation, a quasi-linear variation is verified. The calculated β values are within the range $\beta = 12000$–$1500\,\mathrm{m^{-1}}$, that means a very large accentuation of field emission, in accordance with the literature.[19] Such values should not be

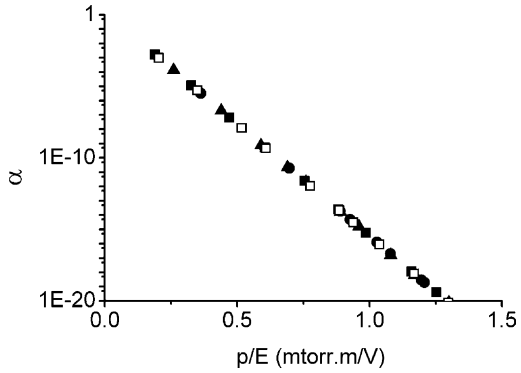

Fig. 8. First ionisation factor α against pressure to electric field ratio for all samples.

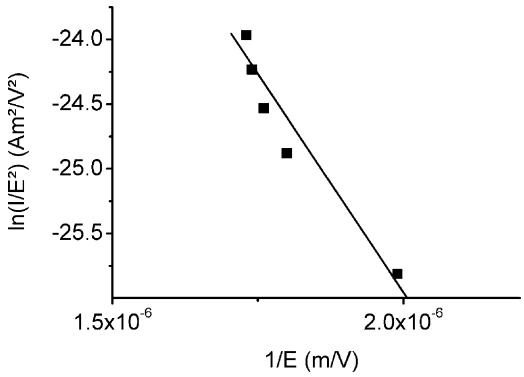

Fig. 9. Fowler–Nordheim plot before and after the breakdown point for the 61 vol.% sample.

only justified by geometrical factors at grains edges, but alternatively they seem to be due to local surface features as locally bonded oxide or various materials.

5. Conclusion

Electrical discharge at surface of SiC-β′-SiAlON granular composite materials are supposed to be originated from two mechanisms. First, if it is assumed that discharge is located at SiC grains boundaries, the Paschen's law can be applied and the percolation of discharge current should be obtained between external electrodes. Some restrictions to this mechanism appear with the very low variation of the breakdown voltage to a large range of pressure. In that case, the primary ionisation coefficient α decreases sharply with pressure and the secondary ionisation coefficient γ attains very unusual values. An additional mechanism of field emission between thin grain boundaries is then supposed and described with the Fowler–Nordheim's law. In that case, the key observation is the very high values of the field emission factor β. It suggests that if air ionisation occurs at the material surface under low electric field, it is highly improved by some SiC surface features as protuberances and physico-chemical local modifications. During the final stage of electrical discharges, both mechanisms suggest that not only the grain boundaries of SiC grains, but the most part of the air atmosphere just above the composite surface is ionised.

References

1. Poorteman, M., Descamps, P., Cambier, F., Plisnier, M., Canonne, V. and Descamps, J. C., Silicon nitride/silicon carbide nanocomposite obtained by nitridation of SiC: fabrication and high temperature mechanical properties. *J. Eur. Soc.* 2003, **23**, 2361–2366.
2. Liu, Q., Gao, L., Yan, D. S. and Thompson, D. P., Hard sialon ceramics reinforced with SiC nanoparticles. *Mat. Sci. Eng.* 1999, **A269**, 1–7.
3. Hu, W., Guan, H., Sun, X., Li, S., Fukumoto, M. and Okane, I., Electrical and thermal conductivities of nickel-zirconia cermet. *J. Am. Ceram. Soc.* 1998, **81**(8), 2209–2212.
4. Duran, P., Tartj, J., Capel, F. and Moure, C., *Processing and characterization of a fine nickel oxide/zirconia/composite prepared by polymeric complex solution synthesis* 2003, **23**, 2125–2133.
5. Von Hippel, A. R., *Molecular Science and Molecular Engineering*. The Technology Press of M.I.T. and J. Wiley, New York, 1959, pp. 39–47.
6. Coster, M. and Chermant, J. L., *Précis D'analyse D'images*. Presses du CNRS, 1989.
7. Coster, M. and Chermant, J. L., Image analysis and mathematical morphology for civil engineering. *Cem. Concr. Compos.* 2001, **23**, 133–151.
8. Braithwaite, N. St. J., Introduction to gas discharge. *Plasma Sour. Sci. Tech.* 2000, **9**, 517–527.
9. Vacquié, S., *L'arc Électrique*, ed. CNRS. Eyrolles, 2000.
10. Von Engel, J. D., *Cobine, Gaseous Conductors*. New York, 1958.
11. Ono, T., Sim, D. and Esashi, M., Micro-discharge and electric breakdown in a micro-gap. *J. Micromech. Microeng.* 2000, **10**, 445–451.
12. Torres, J. M. and Dhariwal, R. S., Electric field breakdown at micrometre separations. *Nanotechnology* 1999, **10**, 102–107.
13. Lenzlinger, M. and Snow, E. H., Fowler–Nordheim tunneling into thermally grown SiO_2. *J. Appl. Phys.* 1969, **40**, 278.
14. Porter, L. M. and Davis, R. F., A critical review of ohmic and rectifying contacts for silicon carbide. *Mater. Sci. Eng. B* 1995, **34**(2/3), 83–105.
15. Kazuya, Y., Ayumi, S., Ichiro, O. and Chuhei, O., Modified Fowler–Nordheim field emission formulae from a nonplanar emitter model. *Surf. Sci.* 2002, **520**(1/2), 18–28.
16. Evtukh, A. A., Klyui, N. I., Litovchenko, V. G., Yu, M. L., Korneta, O. B., Puzikov, V. M. *et al.*, Peculiarities of field emission from silicon carbide films. *Appl. Surf. Sci.* 2003, **215**(1–4), 237–241.
17. Dong, C. L., Hyung, S. A., Doo, J. C., Chae, H. W. and Hajime, T., The field emission properties of silicon carbide whiskers grown by CVD. *Surf. Coat. Technol.* 2003, **168**(1), 37–42.
18. Jimenez, M., Noer, R. J., Jouve, G. and Jodet, J. B. B., Electron field emission from large-area cathodes: evidence for the projection model. *J. Phys. D: Appl. Phys.* 1994, **27**, 1038–1045.
19. Cox, B. M., The nature of emission sites. *J. Phys. D: Appl. Phys.* 1975, **8**, 2065–2073.